ISSN 1063-7710, Acoustical Physics, 2025, Vol. 71, No. 2, pp. 190–200. © Pleiades Publishing, Ltd., 2025.

NONLINEAR ACOUSTICS

# Numerical Simulation of Volumetric Ultrasound Heating of Biological Tissue with Surface Cooling

**P. A. Pestova[a, *], A. N. Rybyanets[b], O. A. Sapozhnikov[a], M. M. Karzova[a], P. V. Yuldashev[a], S. A. Tsysar[a], L. M. Kotelnikova[a], I. A. Shvetsov[b], and V. A. Khokhlova[a]**

[a] *Moscow State University, Moscow, 119991 Russia*

[b] *Research Institute of Physics, Rostov-on-Don, 344090 Russia*

**e-mail: pestova.pa16@physics.msu.ru*

Received February 16, 2025; revised February 27, 2025; accepted March 4, 2025

**Abstract**—One of the undesirable effects of using ultrasound for extracorporeal therapy is skin overheating, caused by both ultrasound absorption and contact with the heated surface of the acoustic transducer. To suppress this effect, a forcibly cooled contact medium can be placed between the skin and the irradiating surface. A novel ultrasound applicator implementing this approach has recently been proposed and developed at Southern Federal University. It uses a rectangular piezoelectric transducer bonded to an aluminum plate for volumetric heating of subcutaneous biological tissue. The plate is cooled by circulating cold water through laterally drilled channels. This article presents a numerical algorithm for calculating the three-dimensional temperature field in tissue during the operation of this applicator. The simulation was based on the inhomogeneous heat equation. Experimental acoustic holography data obtained for the developed transducer were used to calculate the heat sources in tissue. An example of heating bovine liver tissue *ex vivo* is considered, with irradiation times ranging from several seconds to several min. The simulation results were compared with experimental data on tissue thermal ablation at an acoustic power of 12 W and an ultrasound frequency of 6.96 MHz. It is shown that the combination of thermal tissue exposure and contact boundary cooling allows for volumetric tissue heating with a temperature maximum at a depth of 8 to 15 mm, while maintaining a negligible temperature change at depths up to 2–3 mm.

**Keywords:** therapeutic ultrasound, cosmetology, numerical simulation, heat equation

**DOI:** 10.1134/S1063771025600172

## INTRODUCTION

Important limitations in the clinical application of ultrasound physiotherapy [1] and noninvasive surgery using high-intensity focused ultrasound (HIFU) [2–4] concern the risk of thermal damage to the skin. In physiotherapeutic procedures using relatively low ultrasound intensities (up to 3 W/cm$^2$) [1, 5, 6], this problem, although rare, remains a potential complication. The risk of skin damage increases with improper placement of the transducer, with increased radiation intensity, prolonged exposure, or insufficient acoustic contact between the transducer and the skin. HIFU technology is characterized by significantly higher intensity levels in the treatment area (hundreds of W/cm$^2$), although focusing of the field allows for reduced intensity levels on the skin [5, 6]. However, when creating volumetric tissue ablation by moving the focus, the problem of skin overheating becomes critical due to the increase in exposure time [2–4].

Skin overheating can occur when both deep and subcutaneous layers of biological tissue are irradiated. Thus, in recent years, HIFU technology has become widespread in aesthetic medicine, in particular, for procedures for tightening the skin of the face and neck (SMAS-lifting) and other areas of the body [4, 7–10]. Clinical SMAS-lifting systems use transducers that operate in the 4–10 MHz frequency range and can be focused at depths from 1.5 to 4.5 mm [4, 7–9]. The transducer generates ultrasound waves that are focused through the matching medium and superficial layers of the skin to a specified depth, where the acoustic energy is absorbed, heating the tissue to 60–70°C, thereby creating discretely located point thermal microcoagulation zones with a volume of about 1 mm$^3$ [8]. During the resorption of coagulated microablations, a reduction in tissue volume occurs, and, as a wound healing reaction, new forms of viscoelastic collagen and elastin begin to be synthesized [11]. As a result, problem areas of tightened and expression wrinkles are reduced. To localize the ultrasound effect at different depths, transducers with different focal lengths are used, and to treat a large surface or volume of tissue, the transducer moves within a specified contour [7, 12, 13]. Therefore, the proce-

dure time increases and there is a risk of tissue overheating during focus progression [2–4].

To protect the skin and the transducer itself, both in SMAS-lifting cosmetic devices and in the case of exposure to deep areas of the human body, cooling with a contact medium between the skin and the HIFU transducer is used [2, 3, 14, 15]. It should be noted that for the therapeutic effect of ultrasound on tissue, in addition to the thermal mechanism, cavitation is also used; in this case, pulse-periodic modes are used and the effects of skin overheating are weakened [16].

Despite the success of using sources with electronic or mechanical movement of the focus in HIFU therapy in tandem with skin cooling for volumetric action on target areas, the development of alternative methods and devices capable of increasing the volume of ultrasound effect, e.g., on subcutaneous tissue layers without moving the focus but while maintaining the intact of the skin, remains an urgent problem. In [17], it was proposed to use the SUPERB (Synchronous Ultrasound Parallel Beam) technology of the Sofwave Medical system (Yokneam, Israel), which applies the unfocused ultrasound effect. The transducer is a linear ultrasound array consisting of seven transducers offset approximately 1.5 mm from each other and excited in sequence. In this case, the thermal effect is localized in discrete zones at the same distances from each other at a depth of 0.5–2 mm in the dermis owing to cooling of the operating element and its neighboring elements. This ensures localization of the effect and protects the skin from burns. Thus, SUPERB, due to selective cooling of elements, can produce discrete, single, small-volume ablations at a given depth in the skin without damaging its surface layer [17]. However, ensuring uniform volumetric effect on subcutaneous tissue layers both for physiotherapy and for more intensive therapeutic effect on the specified subcutaneous areas of the human body at different depths remains unresolved.

Recently, we have developed the model of a plane transducer that can act on relatively large volumes of subcutaneous tissue layers via superposition of the thermal effect of the ultrasound field and surface cooling [18]. By varying such parameters of action as ultrasound frequency and cooling temperature, it is possible to localize the volumetric effect at different depths. Depending on the irradiation amplitude parameters, the ultrasound effect on tissue can produce different effects, including massage, slight heating used in physiotherapy, cavitation, and even thermal ablation of target volumes.

In this study, a numerical algorithm was developed that can simulate heating of a biological tissue sample with an ultrasound beam in tandem with surface cooling. The efficiency of the method was also demonstrated experimentally by *ex vivo* irradiation of a bovine liver sample using the developed transducer. Since existing methods for recording soft volumetric effects on subcutaneous tissue layers are associated with the occurrence of artifacts (e.g., when thermocouples are used to measure temperature) or are characterized by high cost and complexity of implementation (e.g., magnetic resonance thermography), heating modes to tissue thermal ablation temperatures were considered. This made it possible to visualize the results of irradiation in experiment for comparison with numerical calculation data [18].

## FORMULATION OF THE PROBLEM

Using numerical modeling methods, a physical experiment involving irradiation of a sample of bovine liver tissue *ex vivo* was simulated with an ultrasound applicator consisting of a plane radiating piezoelectric plate and an aluminum plate cooling the surface of the sample. The metallized surfaces of a rectangular piezoelectric plate (PP) measuring 25 × 15 × 1 mm served as electrodes and were connected electrically to a high-frequency cable (Fig. 1a). The PP was made of PKR 78 ferroelectric-rigid piezoceramic with a high piezoelectric modulus (325 pC/N), electromechanical coupling coefficient (0.5), and mechanical quality factor (400) with low dielectric losses (loss tangent 0.003) [19]. All these parameters, together with the fine-grained structure, ensure high efficiency of piezoceramics in the continuous high-intensity ultrasound radiation mode. The PP was glued to the aluminum plate (AP) with dimensions of 25 × 40 mm, which in the contact area was a plane-parallel layer 3 mm thick (Fig. 1b). The outer sections of the AP were thickened and channels were drilled in them, through which a cooling liquid circulated—water at a temperature of 14°C (COOL, Fig. 1a).

The acoustic field generated by the transducer was characterized experimentally in a water tank by acoustic holography [20]. In the experiment of *ex vivo* irradiation of bovine liver tissue, the transducer was applied to the sample with the outer side of the aluminum plate (Fig. 1a). Calibration measurements of the field in water and tissue irradiation were done at room temperature. Thus, the initial sample temperature also corresponded to room temperature (23°C), while the temperature at the boundary of its contact with the aluminum plate was maintained at 14°C. The PP operating frequency approximately corresponded to the third harmonic of its antiresonance frequency of 6.96 MHz. The acoustic power corresponded to the experimental conditions and was 12 W, the duration of exposure was 3 and 5 min, the cooling time of the sample after irradiation was 2 min, the parameters of the biological tissue corresponded to the tabular values of bovine liver. During the simulation, it was assumed that cooling of the tissue with an aluminum plate and its heating with ultrasound were turned on simultaneously.

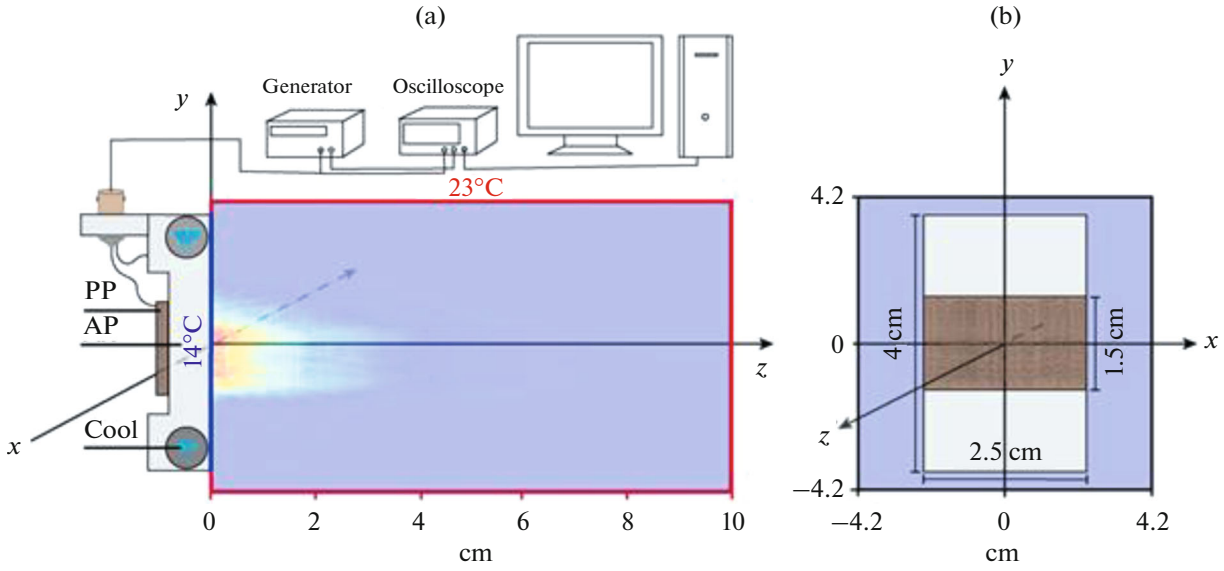


**Fig. 1.** (a) Schematic diagram of the numerical experiment simulating physical *ex vivo* experiment. A plane ultrasound transducer, which was a glued rectangular piezoceramic plate (PP) and an aluminum plate (AP) with channels along its lateral sections (Cool), was applied to a sample of bovine liver with an initial temperature of 23°C. The AP was thermostatted by circulating cold water with a temperature of 14°C through its channels. The spatial distribution of the pressure amplitude of the ultrasound field in the tissue is shown inside the sample. (b) Front view and dimensions of the PP (shown in brown) and cooling AP (shown in gray). The numerical window is shown in blue.

## NUMERICAL MODEL

### *Acoustic Field and Heat Sources*

The propagation of ultrasound waves in water and in a sample of bovine liver sample was described using the angular spectrum method with boundary conditions on the plane of an aluminum plate obtained from experimental data: a pulsed acoustic hologram of the considered ultrasound transducer (Fig. 2) [20, 21]. An acoustic hologram is a recording of the time form of acoustic pressure at the nodes of a square grid on a flat area located at some distance in front of the source and oriented parallel to the transducer. The distance between grid nodes is chosen to be approximately equal to half the wavelength, and the recording area, large enough so that the emitted ultrasound beam is entirely incident on it.

The acoustic hologram measurement was carried out in a water tank with degassed water. A pulse signal in the form of three periods of a sinusoidal signal with a frequency of 7 MHz and an amplitude of 5 V was fed to the transducer from the generator (33250A, Agilent, USA) through an electric power amplifier (210L, Electronics & Innovation, USA). The signal repetition period was 2 ms. The short duration of the emitted pulse signal made it possible to study the field in a fairly wide frequency band present in its spectrum. The acoustic signal was measured using a capsule hydrophone (HGL-0200, ONDA, USA) with a sensitive element diameter of 200 μm. A computer-controlled micropositioning system (UMS-3, Precision Acoustics, UK) allowed the hydrophone to be moved along three mutually perpendicular axes. The pulsed acoustic hologram was recorded at a distance of $z =$ 25 mm from the center of the transducer in a plane perpendicular to its acoustic axis. The field was scanned with a step of 0.2 mm along the transverse coordinates $x$ and $y$ in the nodes of the given 201 × 201 square grid, in a 40.2 × 40.2 mm window. At each hologram node, the signal was recorded for 300 ms, then averaged over 32 samplings to reduce the noise level. The time sampling step was 8 ns. The water temperature was controlled by a thermocouple and was constant 25.1 ± 0.1°C during the hologram measurement. The sound speed at a temperature of 25.1°C was 1479.2 m/s [22].

From the measured time profiles of the hydrophone signal at each point of the spatial grid, the complex spectral signal amplitudes were extracted by Fourier transform at the studied frequencies in the 6.15–7.70 MHz range with a step of 0.01 MHz. After correction taking into account the sensitivity and directivity pattern of the hydrophone, two-dimensional distributions of the complex amplitudes of the acoustic pressure created by the transducer in the hologram measurement plane at the given frequencies were obtained. The distributions were used to calculate the forward and backward propagation of the acoustic field in water. The calculation was carried out using the angular spectrum method. This made it possible to model the acoustic pressure field created by the transducer in water at each of the frequencies considered, as well as the distribution of the pressure amplitude and phase in the plane ($x$, $y$, $z = 0$) containing the radiating surface

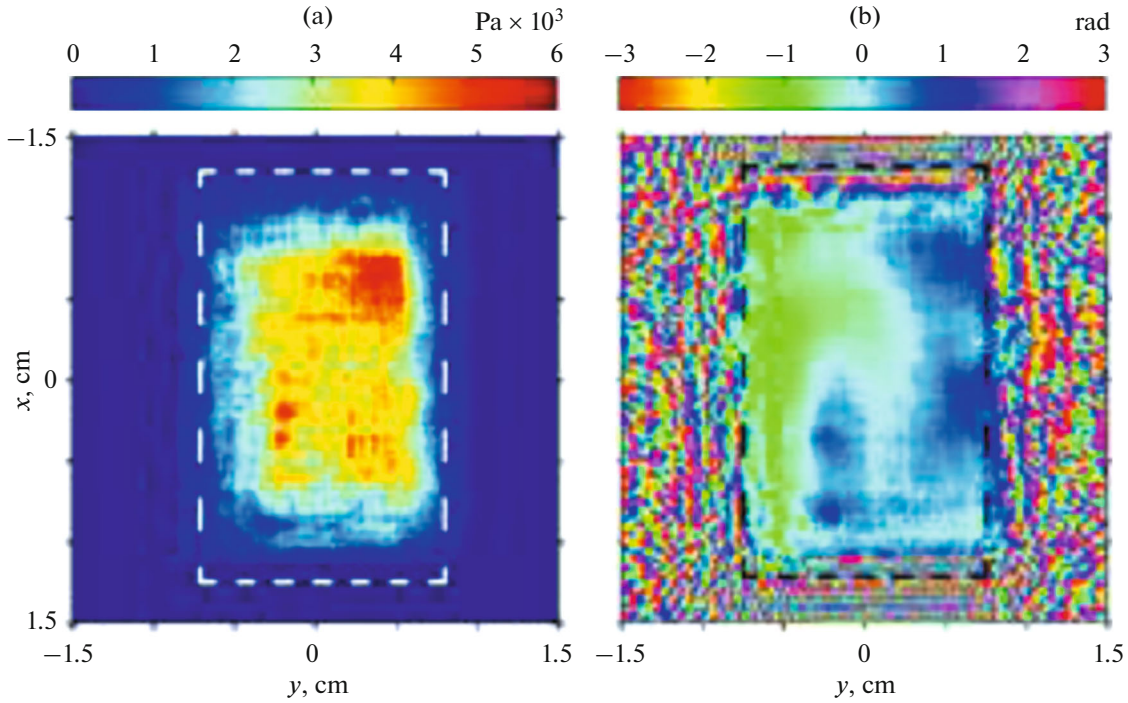


**Fig. 2.** Boundary conditions on the surface of the transducer (the outer surface of the aluminum plate) at $z = 0$, used to simulate the ultrasound field generated in tissue: distributions of (a) amplitude and (b) phase of pressure for an acoustic power of the transducer of 12 W. The dashed lines show the nominal dimensions of the PP 2.5 × 1.5 cm.

of the aluminum plate. The obtained acoustic field distributions were compared to each other in order to select the frequency ensuring the most uniform distribution of the acoustic pressure amplitude both on the surface and in two axial planes of the transducer. As a result, the operating frequency of 6.96 MHz was adopted, and the corresponding acoustic pressure amplitude and phase distributions on the outer surface of the aluminum plate (hereinafter, transducer) were used in the numerical experiment as the boundary conditions for further modeling acoustic field in tissue (Fig. 2). Clearly, the spatial distribution of the pressure amplitude on the transducer differs in size from the nominal dimensions of the PP (Fig. 2, dashed lines), occupying a smaller area. In addition, asymmetry and nonuniformity of distribution are observed: a decrease in amplitude at the edges of the transducer, its increase in the central region, and more pronounced in its upper part.

To set the acoustic power of the piezoelectric transducer used in the experiment (12 W), the obtained pressure amplitude distribution on the transducer plane ($x$, $y$, $z = 0$ mm) was scaled by a factor equal to the square root of the ratio of the specified power to the transducer power calculated from the holographic data. The transducer power was calculated as the integral of the intensity over its surface: $9 \times 10^{-4}$ W at 1 V on the transducer. In the numerical experiment, the power was 12 W. Thus, the amplitude scaling factor was 114.

Using the obtained boundary conditions for the complex amplitude $p_0(x, y, z = 0)$ on the surface of the transducer, the pressure distribution $p(x, y, z)$ was calculated using the angular spectrum method on the entire numerical grid in a propagation medium with the sound speed corresponding to bovine liver tissue. The absorption in the tissue was taken into account by multiplying the propagator by quantity $\exp(-\alpha z)$ [23]:

$$p(x,y,z) = \frac{1}{(2\pi)^2}\int_{-\infty}^{+\infty}\int_{-\infty}^{+\infty} dk_x dk_y S_{p_0}(k_x,k_y,z=0) \times e^{i\sqrt{(\omega/c_0)^2-k_x^2-k_y^2}z} e^{ik_x x+ik_y y} e^{-\alpha z}, \quad (1)$$

$$S_{p_0}(k_x,k_y,z=0) = \int_{-\infty}^{+\infty}\int_{-\infty}^{+\infty} p_0(x,y,z=0) e^{-ik_x x-ik_y y} dxdy, \quad (2)$$

where $S_{p_0}$ is the initial spatial spectrum corresponding to complex pressure distribution $p_0(x,y,z = 0)$ and $k_x$ and $k_y$ are spatial frequencies. Next, when calculating intensity distributions $I(x, y, z) = pp^*/2\rho_0 c_0$ ($p^*$ is the complex conjugate of pressure $p$) and spatial distribution of the power density of heat sources $Q(x, y, z) = 2\alpha I(x, y, z)$ in the inhomogeneous heat conduction equation, the absorption of ultrasound energy in tissue

was taken into account in the plane wave approximation. Here $c_0$, $\rho_0$, and $\alpha$ are the sound speed, density, and attenuation coefficient in bovine liver tissue at the transducer frequency $f_0$. To ensure a constant temperature at the boundary with the cooling plate, an image method was used, consisting of a mirror image of the distribution $Q(x, y, z)$ in the area of negative values $z$ with replacement of the sign:

$$Q(x, y, -z) = -Q(x, y, z). \quad (3)$$

The simulation was carried out for the radiation of a PP at a frequency of $f_0 = 6.96$ MHz; the acoustic parameters of the tissue corresponded to bovine liver: $c_0 = 1580$ m/s, $\rho_0 = 1050$ kg/m$^3$, and $\alpha = 49.78$ m$^{-1}$ [24–26].

### *Temperature Field*

The three-dimensional temperature field in a bovine liver tissue sample *ex vivo*, taking into account its volumetric heating by ultrasound and surface cooling, was calculated using the numerical algorithm developed in the study, which solves the inhomogeneous heat conduction equation:

$$\frac{\partial T}{\partial t} = \chi \Delta T + \frac{Q}{C_v}, \quad (4)$$

where $T = T(x, y, z, t)$ is the temperature in tissue, $t$ is time, $\chi$ is the thermal diffusivity coefficient, $C_v$ is the volumetric heat capacity of the sample, and $Q = Q(x, y, z)$ is the power density of the heat sources in tissue, calculated in the plane wave approximation.

Due to the linearity of Eq. (4), the heating and cooling effects were modeled independently. The solution was presented as a sum:

$$T(x, y, z, t) = T_{\text{sam}} + T_1(x, y, z, t) + T_2(x, y, z, t), \quad (5)$$

where $T_{\text{sam}}$ is the background (initial) temperature of the sample, 23°C; $T_1(x, y, z, t)$ is the solution to the three-dimensional homogeneous heat equation with nonuniform boundary conditions (BCs) corresponding to a constant temperature on the surface of the cooling (aluminum) plate, equal to its difference from the background ($T_1 = T_{\text{cool}} - T_{\text{sam}}$, where $T_{\text{cool}} = 14$°C is the cooling plate temperature) and zero on all other surfaces (Fig. 1a); $T_2(x, y, z, t)$—solution to Eq. (4), describing the change in tissue temperature relative to the background, with uniform BCs ($T_2 = 0$ at the boundaries of the numerical window) and thermal sources $Q$, associated with the absorption of ultrasound beam energy in tissue. This division is due to the fact that for temperature distributions $T_1$ and $T_2$ it is convenient to use various solution methods.

Inhomogeneous heat conduction equation (4) was calculated on a grid consisting of 242 nodes for each of the transverse coordinates $x$ and $y$ with a spatial step of 0.35 mm ($-4.2 \le x(y) \le 4.2$ cm). The size of the simulation area along the beam axis $z$ (axial direction) varied depending on the problem being solved: a grid of 1001 nodes with a step of 0.1 mm ($0 \le z \le 10$ cm was used to simulate the cooling process), whereas for the heating simulation, the size of the axial domain was doubled to ensure uniform boundary conditions at the boundaries of the numerical window (2001 nodes, step 0.1 mm, $-10 \le z \le 10$ cm). The values of the physical parameters corresponded to liver tissue: $\chi = 1.93 \times 10^{-7}$ m$^2$/s, $C_v = 5 \times 10^6$ J/(m$^3$ °C) [25, 26].

### *Sample Cooling Calculation*

To calculate the cooling effects, it was assumed that the temperature on the surface of the aluminum plate was kept constant, $T_{\text{cool}} = 14$°C. The initial background temperature of the biological tissue sample and the temperature at its boundaries, except for the surface of the aluminum plate, was $T_{\text{sam}} = 23$°C (Fig. 1a). The process of cooling a tissue sample relative to the temperature $T_{\text{sam}}$ described by the variable $T_1$, the equation, the initial and boundary conditions for which, taking into account (4) and (5), can be written as

$$\frac{\partial T_1}{\partial t} = \chi \Delta T_1;\ T_1(x, y, z, 0) = 0;\quad T_1(x, y, 0, t) = T_0(x, y)\theta(t), \quad (6)$$

where $T_0(x, y) = \delta T = (T_{\text{cool}} - T_{\text{sam}}) = -9$°C for $-\frac{L_x}{2} \le x \le \frac{L_x}{2}$, $-\frac{L_y}{2} \le y \le \frac{L_y}{2}$, i.e., inside the surface of the aluminum plate and 0 outside; $L_x = 25$ mm, $L_y = 40$ mm are the plate dimensions; $\theta(t)$ is the Heaviside function.

The solution to problem (6) can be written as an inverse two-dimensional Fourier transform of the solution in the -space for each component of the spatial spectrum of the transducer [27]:

$$T_1(x, y, z, t) = \frac{1}{(2\pi)^2} \times \int_{-\infty}^{+\infty}\int_{-\infty}^{+\infty} dk_x dk_y S_{T_1}(k_x, k_y, z, t) e^{ik_x x + ik_y y}, \quad (7)$$

where is the spatial spectrum $S_{T_1}(k_x, k_y, z, t)$ for a rectangular transducer has an exact analytical solution:

$$S_{T_1}(k_x, k_y, z, t) = \frac{\delta T}{2} L_x L_y \text{sinc}\left(\frac{k_x L_x}{2}\right)\text{sinc}\left(\frac{k_y L_y}{2}\right) \times \left\{ e^{-z\sqrt{k_x^2 + k_y^2}}\left[1 + \text{erf}\left(\sqrt{\chi t}\sqrt{k_x^2 + k_y^2} - \frac{z}{\sqrt{4\chi t}}\right)\right] + e^{z\sqrt{k_x^2 + k_y^2}}\left[1 - \text{erf}\left(\sqrt{\chi t}\sqrt{k_x^2 + k_y^2} + \frac{z}{\sqrt{4\chi t}}\right)\right]\right\}. \quad (8)$$

Here $\mathrm{sinc}(x) = \sin x/x$, $erf(z) = \frac{2}{\sqrt{\pi}}\int_0^z e^{-x^2}dx$ is the error function.

Solution (7)–(8) for the function $T_1(x, y, z, t)$ describes the change over time in the spatial distribution of temperature in the tissue volume due to cooling by an aluminum plate with the ultrasound transducer turned off. In the limiting case of long cooling times, a stationary temperature distribution is established in the tissue.

### *Sample Heating Calculation*

The distribution of the temperature field in the tissue during its heating due to absorption of the ultrasound beam energy was calculated by numerically solving the inhomogeneous heat conduction equation with homogeneous boundary conditions:

$$\frac{\partial T_2}{\partial t} = \chi\Delta T_2 + \frac{Q}{C_v};\ T_2(x,y,z,0) = 0;\quad T_2\big|_{\text{boundary}} = 0, \tag{9}$$

where $T_2(x, y, z, t)$ describes the difference in tissue temperature with respect to the background (initial) temperature $T_{\text{sam}} = 23$°C without cooling; $T_2\big|_{\text{boundary}}$ is the tissue temperature at the boundaries of the numerical window (Fig. 1), and $Q(x, y, z)$ are the spatial distributions of the power density of antisymmetric thermal sources, specified by relation (3). After the end of irradiation, the sample cooling process was simulated for 2 min to take into account ongoing heat diffusion.

Problem (9) has an analytical solution in the $k$-space [28]:

$$S_{T_2}(k_x,k_y,k_z,t) = \frac{S_Q(k_x,k_y,k_z)}{\left(k_x^2+k_y^2+k_z^2\right)\chi C_v}\left(1-e^{-\left(k_x^2+k_y^2+k_z^2\right)\chi t}\right), \tag{10}$$

$$S_Q(k_x,k_y,k_z) = \int_{-\infty}^{+\infty}\int_{-\infty}^{+\infty}\int_{-\infty}^{+\infty} dxdydzQ(x,y,z)e^{-ik_xx-ik_yy-ik_zz}, \tag{11}$$

where $S_Q(k_x, k_y, k_z)$ and $S_{T_2}(k_x, k_y, k_z, t)$ are spatial Fourier spectra of $Q(x, y, z)$ and $T_2(x, y, z, t)$. Next, the temperature distribution $T_2(x, y, z, t)$ was calculated as the inverse Fourier transform of analytical solution (10):

$$T_2(x,y,z,t) = \frac{1}{(2\pi)^3} \times \int_{-\infty}^{\infty}\int_{-\infty}^{\infty}\int_{-\infty}^{\infty} dk_xdk_ydk_zS_{T_2}(k_x,k_y,k_z,t)e^{ik_xx+ik_yy+ik_zz}. \tag{12}$$

Thus, solution (12) of system of equations (9) for the function $T_2(x, y, z,t)$ describes the change over time in the spatial distribution of temperature in the tissue volume due to absorption of ultrasound radiation energy at a constant temperature at the sample boundaries. The final distribution of the temperature field of the sample, combining ultrasound heating and surface cooling, is described by the sum of solutions $T_1(x, y, z, t)$, $T_2(x, y, z, t)$, and $T_{\text{sam}}$.

### *Thermal Dose*

The value of the thermal dose was used as the criterion for achieving thermal tissue necrosis:

$$t_{56.0} = \int_0^{t_{\text{heat}}} R_0^{56.0-T(x,y,z,t)}dt \geq 1.76, \tag{13}$$

where the coefficient $R_0$ takes the value 0.5 at $T(x, y, z, t) \geq 43$°C and 0.25 at $T(x, y, z, t) < 43$°C [29]; $t_{56.0}$ is the time equivalent of the threshold destructive thermal dose commonly used in HIFU modes, 240 min at a temperature of 43°C and 1.76 s for a temperature of 56°C [30–32].

## RESULTS

### *1. Acoustic Field in water*

Figure 3 shows the spatial distributions of the pressure amplitude in water in the axial planes $xz$ and $yz$, passing through the center of the transducer for real and ideal transducers with a frequency of 6.96 MHz and an acoustic power of 12 W. For the real transducer used in the experiments (Fig. 3a), boundary conditions were used obtained from experimental acoustic holography data (Fig. 2). In the case of an ideal transducer (Fig. 3b), a uniform distribution of the amplitude of the oscillatory velocity perpendicular to its surface with dimensions corresponding to the nominal dimensions of the PP 2.5 × 1.5 cm and with the same total power of 12 W was assumed.

A comparative analysis of the results of modeling the acoustic pressure field obtained for real and ideal rectangular transducers (Fig. 3) revealed significant differences. The pressure amplitude distributions for an ideal transducer are symmetrical with respect its axis and are characterized by larger beam sizes along both coordinates $x$ and $y$ and approximately twice as small absolute values of the pressure amplitude compared to the field generated by the PP. Although the radiation at the selected frequency of 6.96 MHz near the third harmonic of the fundamental frequency of the PP is characterized by the most uniform and symmetrical pressure distribution among the studied frequencies, the spatial structure of the field of the real transducer remains nonuniform and asymmetrical with respect to its axis ($x = 0$, $y = 0$, $z$). The discrepancy between the nominal dimensions of the radiating surface of the PP and the effective dimensions of the real transducer also manifests itself in the suppression of radiation in its edge regions (Fig. 2). Thus, the use

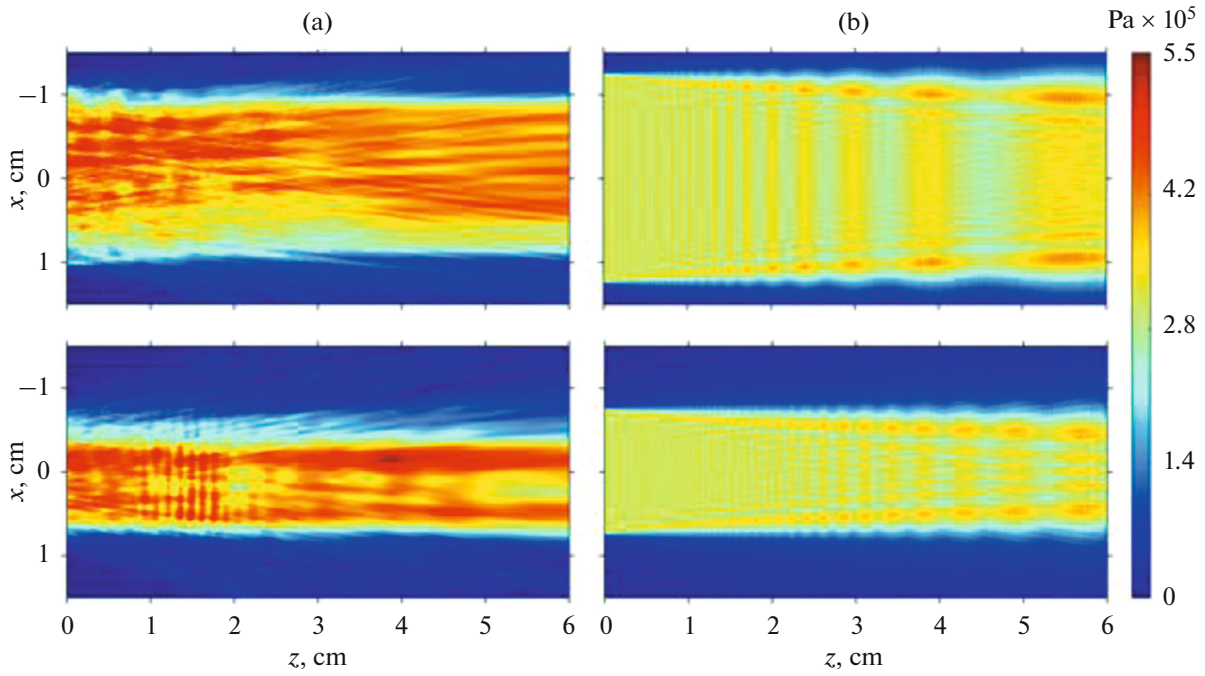


**Fig. 3.** Spatial distributions of pressure amplitude in water in two axial planes *xz* (top line) and *yz* (bottom line) at a frequency of 6.96 MHz for an acoustic power of the transducer of 12 W. The distributions are calculated based on acoustic holography data (a) for the transducer considered and (b) for an ideal piston transducer with nominal dimensions.

of the ideal piston radiator model as an approximation of a real radiator seems incorrect. In this case, the use of experimental data from acoustic holography allows us to obtain boundary conditions that correspond to the conditions of a physical experiment.

### *2. Acoustic Field in Tissue and Heat Sources*

Fig. 4 shows the spatial distributions of the acoustic pressure amplitude calculated numerically in the tissue of a bovine liver sample in planes containing the transducer axis: *xz* at $y = 0$ and *yz* at $x = 0$. The simulation was carried out based on the boundary conditions (Fig. 2) obtained from the measured acoustic hologram for a frequency of 6.96 MHz and an acoustic transducer power of 12 W. As follows from the exponential dependence of the solution (1) along the axis *z*, the characteristic penetration depth of the ultrasound field, determined by the level of the decrease in the amplitude of the pressure wave in *e* once, located at a depth of $1/\alpha$, equal to about 2 cm. At this depth, the maximum value of the pressure amplitude decreases from $6.9 \times 10^5$ to $2.5 \times 10^5$ Pa.

In the specified depth range, effective absorption of acoustic energy by biological tissue occurs, followed by its conversion into thermal energy, which leads to an increase in tissue temperature. Figure 5 shows the corresponding power density distributions of antisymmetric thermal sources in two axial planes *xz* and *yz*: clearly, the effective heating depth $1/2\alpha$ at which the power of heat sources decreases by *e* times, is about 1 cm. However, with prolonged heating (several min), thermal diffusion effects play a major role and therefore it can be expected that the tissue temperature will increase at greater depths. Recall that the antisymme-

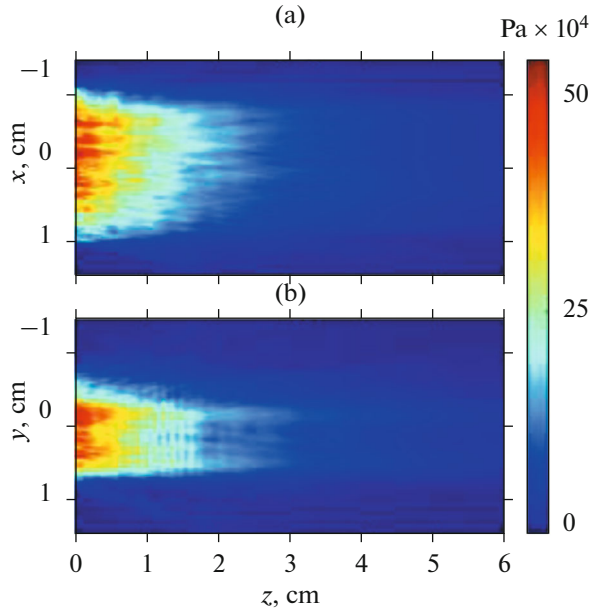


**Fig. 4.** Numerically calculated spatial distributions of pressure amplitude in tissue in axial planes (a) *xz* and (b) *yz* for a frequency of 6.96 MHz and an acoustic power of the transducer of 12 W.

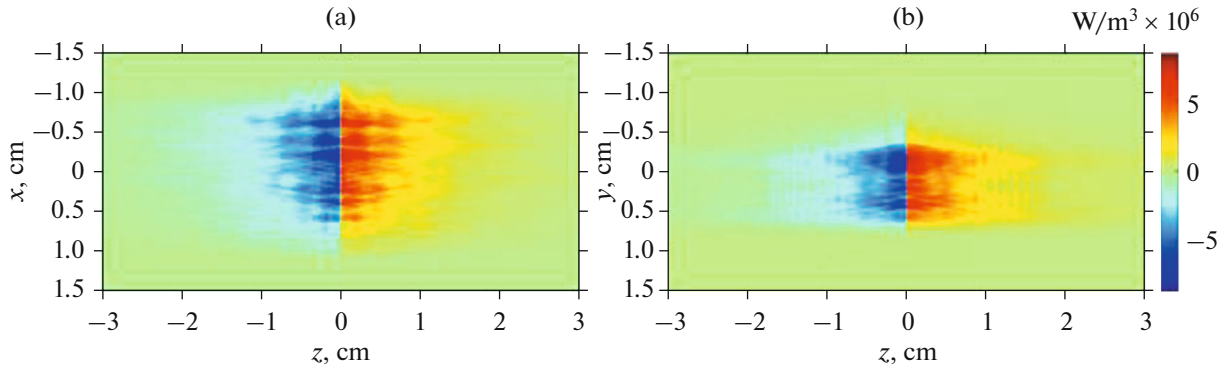


**Fig. 5.** Spatial distribution of the power density of antisymmetric heat sources $Q$ in tissue in axial planes (a) $xz$ and (b) $yz$ at an operating frequency of 6.96 MHz for a transducer power of 12 W.

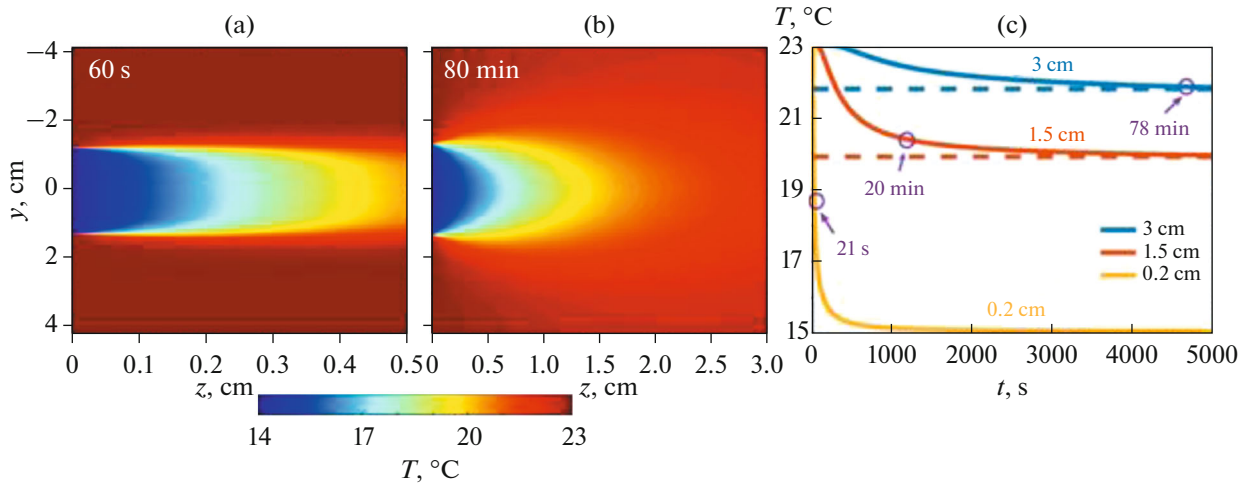


**Fig. 6.** Spatial temperature distributions in tissue (a) at time $t = 60$ s after switching on the sample cooling and (b) after establishment of a stationary temperature distribution at the time $t = 80$ min. (c) Dependences of sample temperature $T$ from time $t$ on the transducer axis for characteristic depths: 3 cm (blue curve), 1.5 cm (red curve), 0.2 cm (yellow curve).

try of heat sources applied in the numerical model (Fig. 5) ensures that a constant temperature is maintained at the boundary $z = 0$.

### *3. Sample Cooling with an Aluminum Plate*

Figure 6 shows the results of solving problem (6)–(8) of surface cooling of a bovine liver sample with an aluminum plate without ultrasound exposure. Two-dimensional temperature distributions are shown in the plane of the transducer axis $yz$ (at $x = 0$) at different moments of time (60 s and 80 min) and the time dependence of the temperature on the transducer axis ($x = 0$, $y = 0$) for three characteristic depths in the tissue: 2 mm, 1.5, and 3 cm.

Figure 6a shows the characteristic spatial distribution of temperature in the biological tissue in the plane of the transducer axis at a time of 60 s. For longer exposure times (about 80 min), a stationary temperature distribution is established in the sample (Fig. 6b). At the same time, as the figure shows, the aluminum plate effectively cools the biological tissue sample at a depth of up to 0.5 cm. At depths from 0.5 to 2 cm, its contribution is less significant, and further on, it is almost completely absent. It should be noted that the surface layers up to 0.2 cm are of primary interest for practical applications in cosmetology [4, 17].

A rough analytical estimate of the time $\tau$ to achieve a stationary temperature distribution at depth can be obtained with simplified normalization of Eq. (4) as $\tau \approx d^2/\chi$ [33]. Estimates for the three characteristic depths of 0.2, 1.5, and 3 cm yield values of $\tau = 21$ s, 20, and 78 min, respectively. Such an estimate of the time to achieve $\tau$ a stationary temperature is of practical interest for preliminary surface cooling, e.g., for anesthesia. Figure 6c plots the time dependence of temperature on the transducer axis for the specified depths of 0.2 cm (yellow curve), 1.5 cm (red curve), and 3 cm

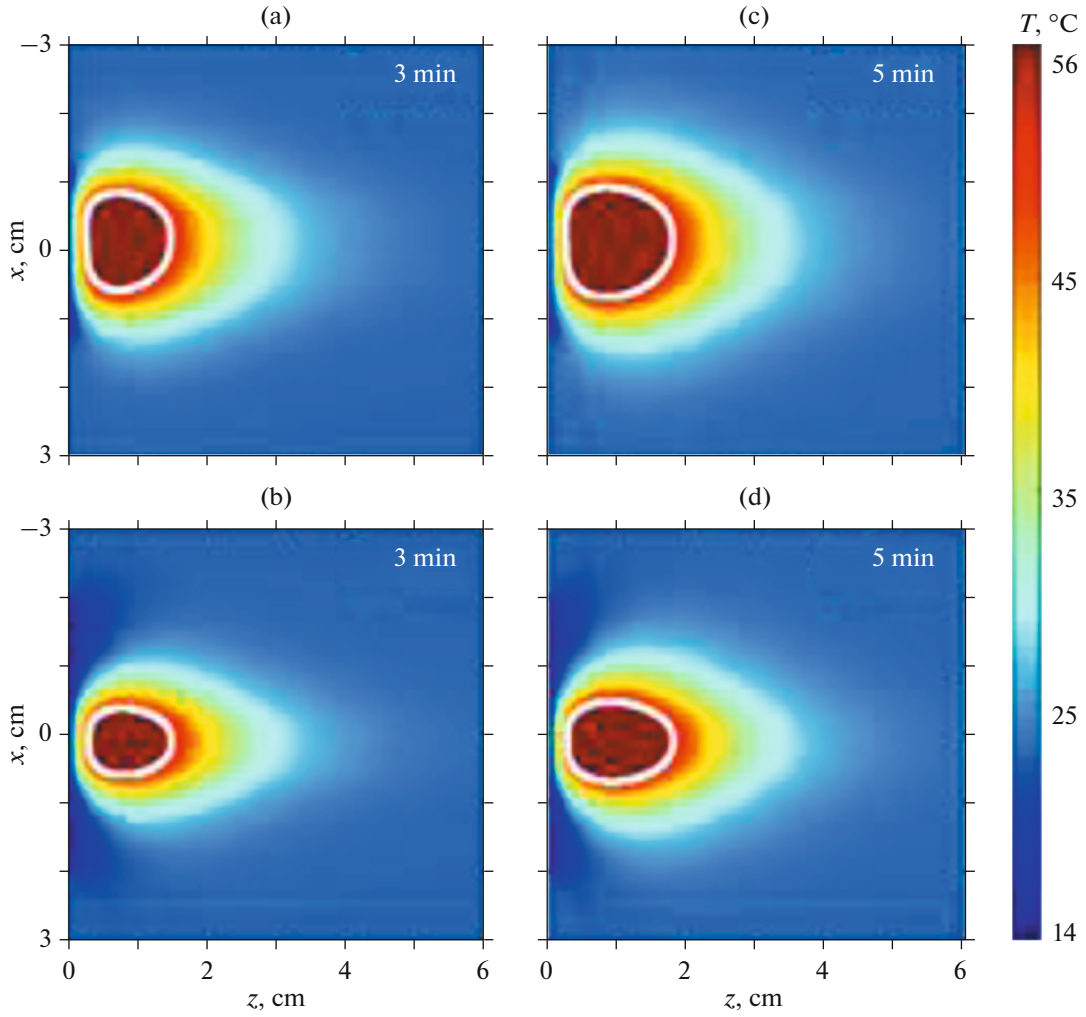


**Fig. 7.** Spatial temperature distributions in axial planes (a, c) *xz* and (b, d) *yz* at the end of the irradiation of a sample of bovine liver with a combination of heating and cooling. The tissue irradiation time was (a, b)—$t = 3$ min and (c, d)—$t = 5$ min. The white outline shows the region within which the thermal dose exceeded the threshold value after the sample had cooled for 2 min.

(blue curve). The estimated time to achieve the $\tau$ values for the corresponding depths are indicated by arrows. Establishment a stationary temperature corresponds to the saturation mode; i.e., the graph reaches a plateau (dashed lines). The graphs in Fig. 6c show that it is possible to cool the tissue at a depth of 0.2 cm to a temperature of 15°C; at a depth of 1.5 cm, to 19.8°C; and at a depth of 3 cm, to 21.8°C. In this case, the analytical estimate of the time $\tau$ agrees well with the simulation results for large depths with an error no greater than 10%. At shallow depths, there is a significant temperature gradient, which requires correction to the coefficient determines the characteristic scale of its change. However, within the error limits, the characteristic time to establish a stationary state at a depth of 0.2 cm is about 2 min (Figs. 6a, 6c). The results indicate that precooling of the superficial layers of biological tissue can help reduce the risk of overheating and pain in the patient during the procedure. The duration of precooling should be adjusted depending on the required depth of action (Fig. 6c).

### *4. Volumetric Heating of a Sample with Surface Cooling*

The results of modeling spatiotemporal temperature distributions in a biological tissue sample in two axial planes *xz* and *yz* with simultaneous activation of ultrasound heating and surface cooling are shown in Fig. 7. Temperature distributions are shown for two irradiation times: 3 min (Fig. 7a, 7b) and 5 min (Fig. 7c, 7d).

As can be seen from the figures, the maximum temperature in the bovine liver sample for an exposure time of 3 min is 66°C and is achieved at a depth of 5 mm (Fig. 7a, 7b), and for 5 min, 72°C at a depth of 8 mm (Fig. 7c, 7d). As the irradiation time increases, the volume of tissue in which the thermal dose exceeds its threshold value corresponding to the achievement

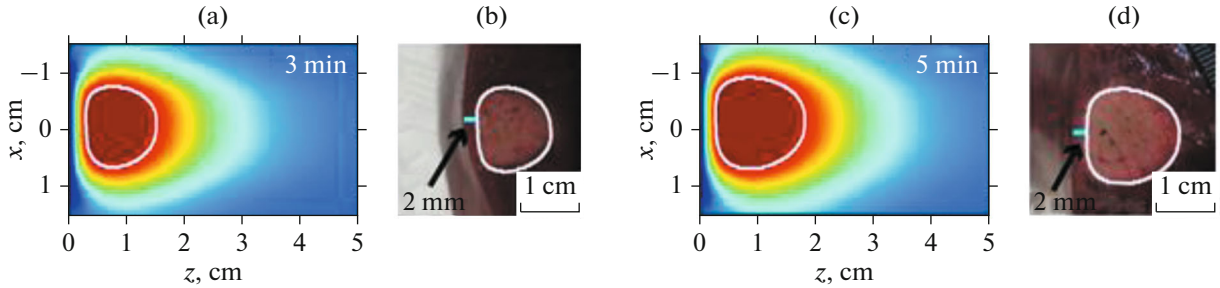


**Fig. 8.** Results of comparing the results of (a, c) numerical and (b, d) physical experiments on ex vivo irradiation of bovine liver tissue for an acoustic power of 12 W and irradiation time of (a, b) 3 and (c, d) 5 min.

of thermal necrosis increases (Fig. 7, the area is outlined in white). The contour of thermal necrosis almost completely coincides with the contour limiting the area where the temperature exceeded 52°C. Thermal ablation has the shape of an oblate spheroid, elongated along the $x$ axis, with dimensions of 1.4 × 0.96 × 1.2 cm for 3 min and 1.5 × 1.2 × 1.5 cm for 5 min (Fig. 7). In both cases, an intact (undamaged) surface layer with nearly the same thickness is observed: 2.8 and 2.7 mm for 3 and 5 min, respectively.

To verify the results of numerical modeling, a comparison was made with the results of physical experiments on thermal ablation of bovine liver tissue *ex vivo* (Fig. 8) [18]. As a result of superposition of volumetric ultrasound heating and surface cooling, thermal ablation was formed in the samples without damage to the surface layer of the liver sample with a thickness of about 2 mm (Figs. 8b, 8d). The shape and dimensions of thermal ablation obtained in numerical modeling showed good qualitative and quantitative agreement with the results of the physical experiment (Fig. 8).

Thus, the results of numerical modeling performed using the described algorithms demonstrate an adequate description of the physical experiment, confirming the operability of the proposed method of volumetric effect on biological tissue with unfocused ultrasound while maintaining its surface layer intact.

## CONCLUSIONS

The paper presents an algorithm for solving the nonuniform bioheat equation that describes the process of volumetric heating of biological tissue under the influence of unfocused ultrasound generated by a plane piezoelectric plate (PP) and cooling of its surface layer.

Analysis of the analytical solution to the problem of volumetric cooling in the absence of ultrasound exposure showed that effective tissue cooling is provided at a depth of up to 5 mm. In this case, the time characteristics for achieving a stationary temperature at depths of 0.2, 1.5, and 3 cm are 21 s, 20 min, and 78 min, respectively. At a depth of 0.2 cm, the maximum cooling in the absence of ultrasound heating is about 8°C (the sample is cooled from the initial temperature of 23 to 15°C) and is achieved within a few min. Thus, to ensure an analgesic effect and protect the 2-mm-thick surface layer before ultrasound exposure, it is recommended to precool the surface of the biological tissue for at least 2 min.

Numerical modeling of the process of obtaining volumetric thermal ablation in a sample of bovine liver, carried out using an unfocused ultrasound beam generated by a PP, in combination with cooling of the surface layers with an aluminum plate, showed the formation of thermal ablation in the form of an oblate spheroid. The threshold thermal dose was exceeded at irradiation times of 3 and 5 min inside a volume with a temperature exceeding 52°C, while the surface layer, the thickness of which was at least 2 mm, remained intact. Qualitative and quantitative compliance shown the comparison of the results of modeling with experimental data allowed us to verify the numerical algorithm presented in this study. The obtained results also demonstrated the potential of using the proposed method to obtain localized volumetric thermal ablation or other ultrasound volumetric effects on the surface layers of biological tissue while maintaining the surface layer intact.

In this study, an example of a specific transducer with fixed parameters was considered. In general, the shape and size of thermal ablation or other ultrasound effect will depend on several factors: the geometry, frequency, and power of the ultrasound transducer, as well as the size and cooling temperature of the aluminum plate. For example, localization of ultrasound exposure at a shallower depth can be achieved by selecting a higher frequency. At low frequencies, the penetration depth of ultrasound will be greater, so the final area of effect will have a larger size in depth. The thickness of the intact layer will depend on the surface cooling temperature. By changing these parameters, it is possible to obtain different shapes and volumes of thermal ablation, which is the subject of further research.

## FUNDING

The study was supported by the Russian Science Foundation (grant no. 24-72-10128, https://rscf.ru/project/24-72-10128/) at Southern Federal University.

## CONFLICT OF INTEREST

The authors of this work declare that they have no conflicts of interest.

## REFERENCES

1. A. M. Enyakov, Al'm. Sovr. Metrol. **3** (4), 152 (2015).
2. C. Mougenot, M. O. Köhler, J. Enholm, B. Quesson, and C. Moonen, Med. Phys. **38**, 272 (2011).
3. S. Crouzet, J. Y. Chapelon, O. Rouviere, F. Mege-Lechevallier, M. Colombel, H. Tonoli-Catez, X. Martin, and A. Gelet, Eur. Urol. **65**, 907 (2014).
4. H. J. Laubach, I. R. Makin, P. G. Barthe, M. H. Slayton, and D. Manstein, Dermatol. Surg. **34** (5), 727 (2008).
5. M. R. Bailey, V. A. Khokhlova, O. A. Sapozhnikov, S. G. Kargl, and L. A. Krum, Acoust. Phys. **49** (4), 369 (2003).
6. G. Haar, Prog. Biophys. Mol. Biol. **93**, 111 (2007).
7. E. J. Ko, J. Y. Hong, T. R. Kwon, E. J. Choi, Y. J. Jang, S. Y. Choi, K. H. Yoo, S. Y. Kim, and B. J. Kim, Skin Res. Technol. **23** (4), 558 (2017).
8. A. M. Al-Jumaily, H. Liaquat, and S. Paul, Ultrasound Med. Biol. **50** (1), 8 (2024).
9. D. Day, Res. Rep. Focus. Ultrasound **2**, 13 (2014).
10. K. A. Gutowski, Clin. Plast. Surg. **43** (3), 577 (2016).
11. G. Oni, R. Hoxworth, S. Teotia, S. Brown, and J. M. Kenkel, Aesthet. Surg. J. **34** (7), 1099 (2014).
12. W. M. White, I. R. Makin, P. G. Barthe, M. H. Slayton, and R. E. Gliklich, Arch. Facial Plast. Surg. **9** (1), 22 (2007).
13. J. L. MacGregor and E. L. Tanzi, Semin. Cutan. Med. Surg. **32** (1), 18 (2013).
14. E. Checcucci, et al., J. Ultrasound **25** (2), 225 (2022).
15. H. J. Lee, M. H. Lee, S. G. Lee, U. C. Yeo, and S. E. Chang, Lasers Surg. Med. **48** (9), 878 (2016).
16. S. A. Brown, L. Greenbaum, S. Shtukmaster, Y. Zadok, S. Ben-Ezra, and L. Kushkuley, Plast. Reconstr. Surg. **124** (1), 92 (2009).
17. W. Hongcharu, K. Boonchoo, and M. H. Gold, J. Cosmet. Dermatol. **22** (5), 1488 (2023).
18. A. N. Rybyanets, I. A. Shvetsov, N. A. Shvetsova, S. A. Tsysar', L. M. Kotel'nikova, V. A. Khokhlova, and O. A. Sapozhnikov, in *Proc. 36th Session of the Russian Acoustical Society* (GEOS, Moscow, 2024), p. 1180 [in Russian].
19. A. N. Rybyanets, I. A. Shvetsov, N. A. Shvetsova, M. A. Marakhovsky, and N. A. Kolpacheva, J. Adv. Dielectr. **15** (3), 2540001 (2025).
20. O. A. Sapozhnikov, S. A. Tsysar, V. A. Khokhlova, and W. Kreider, J. Acoust. Soc. Am. **138** (3), 1515 (2015).
21. D. A. Nikolaev, S. A. Tsysar, V. A. Khokhlova, W. Kreider, and O. A. Sapozhnikov, J. Acoust. Soc. Am. **149** (1), 386 (2021).
22. G. S. Wong and S. Zhu, J. Acoust. Soc. Am. **97** (3), 1732 (1995).
23. C. P. Keravnou, M. -L. Izamis, and M. A. Averkiou, Ultrasound Med. Biol. **41** (11), 3001 (2015).
24. Yu. S. Andriyakhina, M. M. Karzova, P. V. Yuldashev, and V. A. Khokhlova, Acoust. Phys. **65** (2), 141 (2019).
25. F. A. Duck, *Physical Properties of Tissue* (Acad. Press, London, 1990).
26. https://itis.swiss/virtual-population/tissue-properties/database/acoustic-properties/.
27. A. N. Tikhonov and A. A. Samarskii, *Equations of Mathematical Physics* (Nauka, Moscow, 1977) [in Russian].
28. P. A. Pestova, M. M. Karzova, P. V. Yuldashev, W. Kreider, and V. A. Khokhlova, Acoust. Phys. **67** (3), 250 (2021).
29. S. A. Sapareto and W. C. Dewey, Int. J. Radiat. Oncol. Biol. Phys. **10** (6), 787 (1984).
30. *Physical Principles ofMedical Ultrasonics,* Ed. by C. R. Hill, J. C. Bamber, and G. R. ter Haar (Ellis Horwood Ltd., Chichester, 1986; Fizmatlit, Moscow, 2008).
31. X. Fan and K. Hynynen, Ultrasound Med. Biol. **22** (4), 471 (1996).
32. A. M. Venkatesan, A. Partanen, T. K. Pulanic, M. R. Dreher, J. Fischer, R. K. Zurawin, R. Muthupillai, S. Sokka, H. J. Nieminen, N. Sinaii, M. Merino, B. J. Wood, and P. Stratton, J. Vasc. Interv. Radiol. **23** (6), 786 (2012).
33. N. V. Kramarenko, Vestn. Samar. Gos. Tekh. Univ., Ser. Fiz.-Mat. Nauki **25** (1), 163 (2021).